AIP | Applied Physics Letters

Stacking faults and interface roughening in semipolar (20 2 ¯ 1 ¯) single InGaN quantum wells for long wavelength emission

Feng Wu, Yuji Zhao, Alexey Romanov, Steven P. DenBaars, Shuji Nakamura, and James S. Speck

Citation: Applied Physics Letters **104**, 151901 (2014); doi: 10.1063/1.4871512
View online: http://dx.doi.org/10.1063/1.4871512
View Table of Contents: http://scitation.aip.org/content/aip/journal/apl/104/15?ver=pdfcov
Published by the AIP Publishing

Stacking faults and interface roughening in semipolar $(20\bar{2}\bar{1})$ single InGaN quantum wells for long wavelength emission

Feng Wu,[1] Yuji Zhao,[1] Alexey Romanov,[1,2,3,4] Steven P. DenBaars,[1] Shuji Nakamura,[1] and James S. Speck[1]
[1]*Materials Department, University of California, Santa Barbara, California 93106, USA*
[2]*Ioffe Physical-Technical Institute, Russian Academy of Science, St. Petersburg 194021, Russia*
[3]*ITMO University, St. Petersburg 197101, Russia*
[4]*Institute of Physics, University of Tartu, Tartu 51014, Estonia*

(Received 6 March 2014; accepted 4 April 2014; published online 16 April 2014)

The microstructure of InGaN single quantum wells (QWs) grown in semipolar $(20\bar{2}\bar{1})$ orientation on GaN substrates was studied by transmission electron microscopy. Stress relaxation in the lattice mismatch $In_xGa_{1-x}N$ layer was realized by forming partial misfit dislocations associated with basal plane stacking faults (BPSFs). For given composition $x = 0.24$, BPSFs formation was observed when the QW thickness exceeded 4 nm. The high density of partial threading dislocations that bound the BPSFs is detrimental to light-emitting device performance. Interface roughening (faceting) was observed for both upper and lower QW interfaces (more pronounced for upper interface) and was found to increase with the thickness of the QW. BPSFs had a tendency to nucleate at roughened interface valleys. © *2014 AIP Publishing LLC*. [http://dx.doi.org/10.1063/1.4871512]

III-nitride (Al,Ga,In)N heterostructures grown in nonpolar and semipolar orientations are advantageous for the fabrication of quantum wells (QWs) due to the reduction or absence of polarization discontinuities at heterointerfaces—in the case of InGaN QWs this results in reduced or eliminated polarization-related electric fields.[1–5] For example, the semipolar $(20\bar{2}\bar{1})$ plane has attracted considerable attention in the case of blue ($\lambda = 450$ nm) light-emitting diodes (LEDs).[6] For the growth in this particular orientation, the polarization-related electric field and the *p-n* junction built-in electric field are in opposite direction and nearly equal in magnitude that results in a relatively flat QW potential profile during device operation.[7] This feature has been used to produce high efficiency and low droop blue LEDs with relatively thick (~12 nm) QWs.[8] However, a recent atom probe tomography (APT) study indicated that a higher indium composition is required for $(20\bar{2}\bar{1})$ devices to achieve the same emission wavelength than the $(20\bar{2}1)$ devices, due to the absence of polarization-related electric fields in $(20\bar{2}\bar{1})$ QWs in diodes.[9] This potentially make it challenging for the growth of high quality long wavelength $(20\bar{2}\bar{1})$ InGaN QWs. Several other advantageous features, including high optical polarization ratio, small wavelength shift, and narrow spectral linewidth, were also reported on green $(20\bar{2}\bar{1})$ LEDs.[10,11]

The growth of high indium composition InGaN QWs in the nonpolar and semipolar orientation, however, often requires control of misfit dislocation (MD) generation at the QW heterointerfaces as a result of stress relaxation processes.[12–18] For the nonpolar *m*-plane, prismatic plastic slip on inclined *m*-planes leads to the formation of MDs.[17,18] These dislocations have their lines along the *c*-direction and contribute to plastic misfit relaxation in the in-plane *a*-direction. Basal plane stacking faults (BPSFs) were also observed in *m*-plane grown samples and attributed to stress relaxation along the *c*-direction.[12,19] For semipolar growth orientations, more than one possible stress relaxation pathway has been found.[13–16] Mainly, MDs were formed as a result of basal slip system activation[13] via pre-existing threading dislocations bending and gliding on the (0001) plane—these results were supported by cathodoluminescence observations.[14] A second set of MDs was formed by activating dislocation slip on inclined *m*-planes.[15,16] Recently, Wu *et al.* reported on partial strain relaxation related to BPSFs formation in semipolar $(1\bar{1}01)$ grown heterostructures.[20] In the present paper, we report on the results on BPSFs formation and interfacial roughening in semipolar $(20\bar{2}\bar{1})$ InGaN QW heterostructures designed for the long wavelength green LEDs.

LED structures were grown by conventional metal organic chemical vapor deposition (MOCVD) on free-standing semipolar $(20\bar{2}\bar{1})$ GaN substrates supplied by Mitsubishi Chemical Corporation. The device structure consisted of a 1 μm GaN underlayer (with or without Si doping), an $In_{0.24}Ga_{0.76}N$ QW, a 10 nm Mg-doped $Al_{0.15}Ga_{0.85}N$ electron blocking layer (EBL), and a 120 nm *p*-type GaN top layer. The QW thicknesses for the studied samples were 3 nm (sample 1), 7 nm (sample 2), and 10 nm (sample 3). The target emission wavelengths for these devices were in the range of 500–510 nm.

All samples were characterized by transmission electron microscopy (TEM). Electron scattering contrast images were taken with an FEI Tecnai G2 Sphera Microscope operated at 200 kV. High resolution TEM (HRTEM) and high-angle annular dark-field (HAADF) images were taken with an FEI Titan FEG High Resolution TEM/scanning transmission electron microscope (STEM) and Analytical Microscope, operated at 300 kV. APT was performed in laser mode with a Cameca Local Electrode Atom Probe 3000X HR. The sample temperature was about 30 K. A Nd:YAG laser (532 nm second harmonic and 120 ps pulse width) was pulsed at 250 kHz with a pulse energy of 0.06 nJ for the APT experiments. The samples were prepared by focused ion beam (FIB) with a Helios 600 Dual Beam instrument.

There are three widely recognized BPSF types in the wurtzite structure: I_1, I_2, and E, e.g., see Refs. 12 and 21. I_1, I_2 are intrinsic stacking faults, while E is the extrinsic one. I_1-type BPSFs are formed by removing one basal plane and shearing remaining planes by $^1/_3\ \langle 10\bar{1}0\rangle$; the displacement vector **R** associated with this procedure is $^1/_6\ \langle 20\bar{2}3\rangle$ I_2-type BPSFs are formed by only shearing one side planes by $^1/_3\ \langle 10\bar{1}0\rangle$, the displacement vector **R** is therefore $^1/_3\ \langle 10\bar{1}0\rangle$. E-type BPSF is formed by inserting a single wurtzite layer into a perfect crystal, **R** is $^1/_2$ [0001]. In addition, another type of BPSF named I_3 was identified as a combination of two symmetric I_1-type BPSFs.[22]

BPSFs and partial dislocations (PDs) were examined with weak beam dark field (WBDF) electron scattering contrast images, HRTEM and HAADF images. Differing from conventional TEM image, HAADF image is acquired in higher angles. The contrast in HAADF image is mainly related to atomic number of specimen. InGaN is brighter than GaN in HAADF images due to the higher scattering power. On the other hand, WBDF is used to image the dislocation lines and determine the Burgers vectors. A much higher resolution of strained regions around defects can be obtained using WBDF method, which is preferable for dislocation analysis. The invisibility criterion for BPSFs in scattering contrast images gives $\mathbf{g}\cdot\mathbf{R}$ equals to zero or integer. For PDs, the approximate invisibility criterion is $\mathbf{g}\cdot\mathbf{b}=0$ (where **b** is the dislocation Burgers vector). The diffraction vectors used in this study included $\mathbf{g}=0002$, $\mathbf{g}=\{10\bar{1}0\}$, $\mathbf{g}=\{10\bar{1}1\}$, and $\mathbf{g}=\{11\bar{2}0\}$. BPSFs are out of contrast in $\mathbf{g}=0002$ and $\mathbf{g}=\{11\bar{2}0\}$, and only show contrast in $\mathbf{g}=\{10\bar{1}0\}$ and $\mathbf{g}=\{10\bar{1}1\}$. The types of PDs bounding with I_1- and I_2-types BPSFs are different. The Burgers vectors of PDs bonding with I_1-type BPSFs are $^1/_6\ \langle 20\bar{2}3\rangle$. This kind of PD shows contrast in $\mathbf{g}=0002$ diffraction condition. The Burgers vectors of PDs bounding the I_2-type BPSFs are $^1/_3\ \langle 10\bar{1}0\rangle$. This kind of PDs is out of contrast in $\mathbf{g}=0002$. The TEM study revealed that the density of extended defects in the sample increased with the increasing QW thickness. Very few defects were observed for the sample with 3 nm QW. When the QW thickness increased to 4 nm, BPSFs started to form. The density of BPSFs in the order of $10^5\ \mathrm{cm}^{-1}$ was observed for samples with QWs thicker than 6 nm.

Figure 1 presents the HAADF images of $(20\bar{2}\bar{1})$ grown LED structure with a 3 nm InGaN QW (sample 1). The contrast of the InGaN QW appears uniform; the surface of sample was flat in low magnification as shown in Fig. 1(a). However, the upper and lower interfaces of the InGaN QW have atomic scale roughness as shown in Fig. 1(b). The lower interface has only a slight tendency for facet formation, while visible $(10\bar{1}0)$ and $(10\bar{1}\bar{1})$ facets formed at upper interface. The length of facets is 2–4 nm, and the amplitude of interface roughness is less than 1 nm. There are no dislocations and planar defects observed at this QW thickness.

Figure 2 presents the WBDF images for sample 2 with a 7 nm thick QW. Figure 2(a) is the $[\bar{1}2\bar{1}0]$ cross-sectional image taken under $\mathbf{g}=10\bar{1}0$ diffraction conditions. Most of the BPSFs extend to the sample surface. The intersection of the BPSFs with the free surface causes a morphological instability. Some of BPSFs end with GaN cap layer are marked with an arrow in Figs. 2(a)–2(c). The PDs bounding

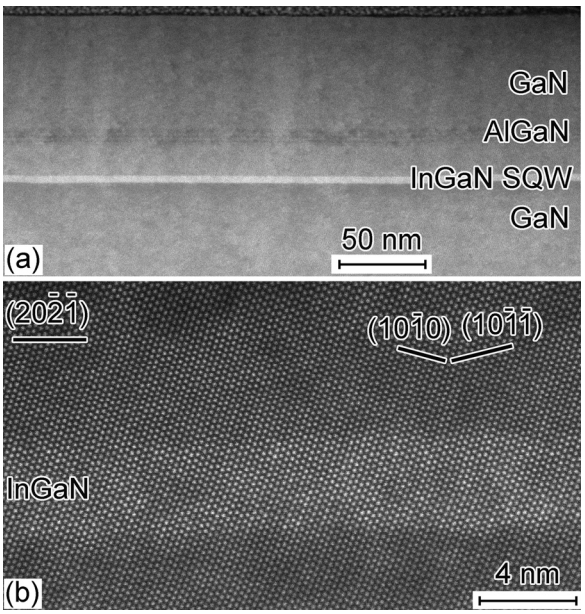

FIG. 1. $[\bar{1}2\bar{1}0]$ cross-sectional HAADF images of semipolar $(20\bar{2}\bar{1})$ LED structure with a 3 nm InGaN QW (sample 1). (a) HAADF image of the whole LED structure. (b) HAADF image of InGaN QW on atomic scale. The zigzag upper and lower surfaces are mainly composed of $(10\bar{1}0)$ and $(10\bar{1}\bar{1})$ facets.

this kind of BPSFs show strong contrast under diffraction condition with $\mathbf{g}=0002$ or $\mathbf{g}=10\bar{1}\bar{1}$ (not shown), suggesting that the BPSFs are of I_1-type. Figure 2(b) is the $[10\bar{1}4]$ cross-sectional image taken in $\mathbf{g}=10\bar{1}0$ near the [0001] zone axis. From this image, it can be seen that the final shape of

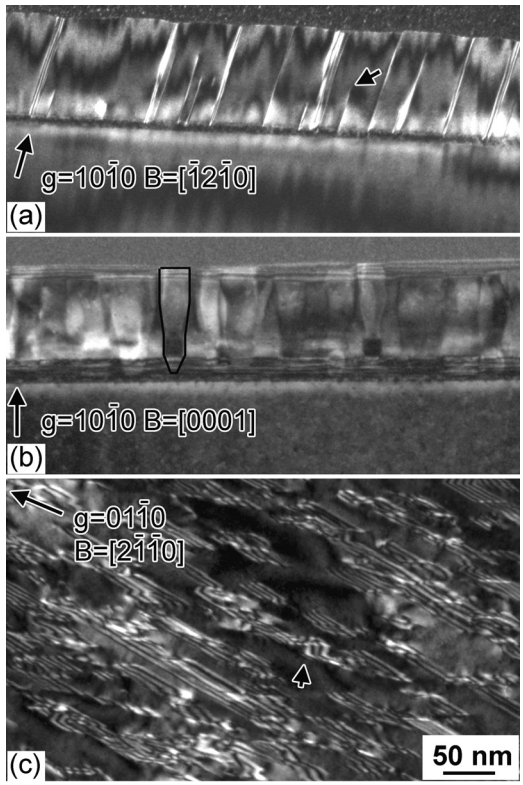

FIG. 2. WBDF images of BPSFs in semipolar $(20\bar{2}\bar{1})$ LED structure with a 7 nm InGaN QW (sample 2). (a) Image is taken from $[\bar{1}2\bar{1}0]$ cross-section sample. (b) Image is taken from $[10\bar{1}4]$ cross-section sample. (c) Image is taken from plane-view TEM sample.

BPSFs is like a narrow U as is highlighted in Fig. 2(b). Figure 2(c) is the plane-view image of the same sample. The sample was tilted to the $[2\bar{1}\bar{1}0]$ zone axis to realize $\mathbf{g}=01\bar{1}0$ diffraction conditions. The average width of BPSFs is about 50 nm and average spacing is about 30 nm. It was also observed that BPSFs can fold into $\{11\bar{2}0\}$ prismatic plane and then fold back to another basal plane, which is marked by an arrow in the image. The density of threading PDs was estimated to be on the order of $10^{10}\,\mathrm{cm}^{-2}$, due to the presence of short and dense BPSFs. This high dislocation density is extremely detrimental to the device performance. Note that the initial threading dislocation density for $(20\bar{2}\bar{1})$ GaN substrate was on the order of $10^{6}\,\mathrm{cm}^{-2}$, which is four orders of magnitude lower than the observed PD densities. Therefore, the short BPSFs and PDs were not related to substrate threading dislocations.

Figure 3 presents HAADF image for 10 nm thick InGaN QW layer of sample 3. For this sample, BPSFs were generated with an average spacing of about 30 nm. Most of the BPSFs examined were I_1-type as marked with inclined "T" in Fig. 3(a). Note that the BPSFs terminated within the InGaN layer, usually at the region from 5 to 6 nm above the lower interface. The interface roughening in this thickness QW becomes more obvious. The dark V-shape areas correspond to the roughened interface valleys. Most BPSFs nucleated at these locations; one such event is circled and highlighted in Fig. 3(a). Figure 3(b) is a high resolution HAADF image. The area marked with an arrow clearly documents one basal plane removal. The inset in Fig. 3(b) shows a HRTEM is taken from the surface of this BPSF, the stacking sequence indicates that the BPSF is of I_1-type. Figure 3(c) is HAADF image taken in lower magnification. The QW region showed inclined stripe contrast in an orientation parallel to the traces of $(20\bar{2}3)$ and $(10\bar{1}1)$ planes. The origin of this contrast in the QWs is unresolved but is possibly due to strain or composition fluctuations. APT studies (not shown) showed that the thin QW samples had indium composition distributions that followed a binomial distribution, which is expected for a random alloy, whereas the thick QW samples showed deviations from the binomial distribution, which indicate compositional clustering. The reconstructed APT data sets also showed evidence of QW thickness fluctuations as observed by cross-section TEM. The indium content of the QWs, for the thicker well samples was 18%. Thus, indium composition fluctuations or clustering, beyond those expected for a random alloy, were observed in the thick QW samples and are a likely cause of the QW stripe contrast in Fig. 3(c).

It was mentioned above that the roughed interfaces of InGaN layer are composed of $(10\bar{1}0)$ and $(10\bar{1}\bar{1})$ facets. These planes, i.e., $(10\bar{1}0)$ and $(10\bar{1}\bar{1})$, of wurtzite crystal structure are energetically more stable compared to $(20\bar{2}\bar{1})$ plane, especially $\{10\bar{1}1\}$ family are often observed as facets in III-nitride compounds and form the sidewalls of "V-defects."[23,24] These two observed facet types are close in their crystallographic orientation to $(20\bar{2}\bar{1})$ plane. In addition, it is also well known, that the transition to a wavy surface contributes to stress relaxation in elastically strained layers.[25] There is an interplay between surface energy increase due to the increase of the area and the diminishing of the stored elastic energy, which provides the stability of rough (wavy) surface.

The critical thickness for MD formation in semipolar $(20\bar{2}\bar{1})$ grown $In_xGa_{1-x}N$/GaN heterostructures was calculated in the framework of Matthews-Blakeslee approach; see Ref. 25 for the background of the approach and Ref. 26 for its realization in semipolar grown III-nitride heterostructures. Two cases were analyzed, as it is given in Fig. 4: the formation of partial MDs that bound BPSFs of I_1-type and the formation of complete lattice MDs that originated from basal plane slip. Calculations showed that the surface energy γ_{SF} of BPSFs practically does not influence the magnitude of the critical thickness in the range of the reported values of $\gamma_{SF}=0.025\,\mathrm{J/m}^2$.[22] The critical thickness for the formation of partial MDs is lower in all cases when compared to the basal plane MDs, which is a consequence of the steep inclination of the basal plane in this particular semipolar heterostructure and corresponding diminishing of the force acting on dislocations gliding in the basal plane. For given In composition $x=0.18$ of $In_xGa_{1-x}N$ QW, we have estimated the critical thickness h_c for the formation of partial misfit dislocations associated with BPSFs on the order of a several nm—consistent with the observation of BPSF formation in the thicker

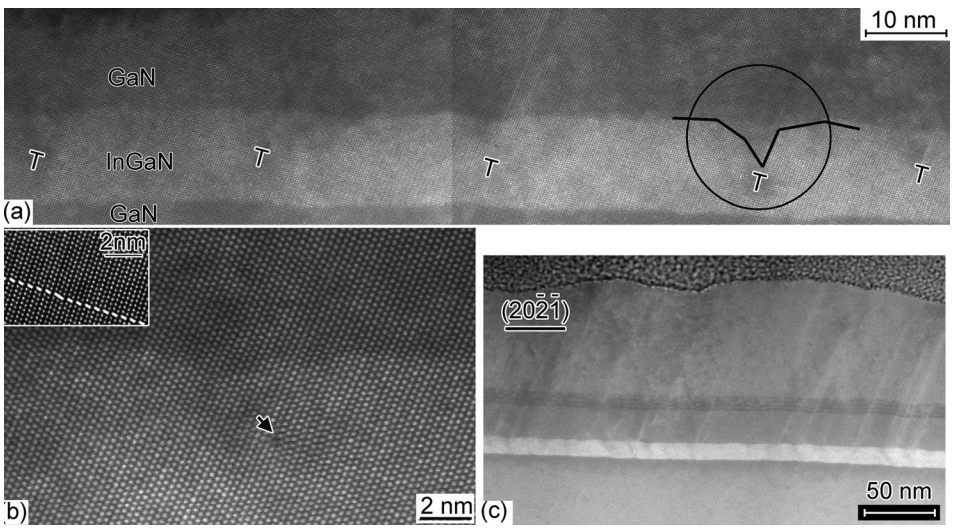

FIG. 3. $[\bar{1}2\bar{1}0]$ cross-sectional HAADF images of semipolar $(20\bar{2}\bar{1})$ LED structure with a 10 nm InGaN QW (sample 3). (a) Image of InGaN layer, the BPSFs with one layer removal are marked. (b) Enlarged image of one BPSF in image (a), the arrow shows the one atomic layer, which is removed. Inset: HRTEM image of this stacking fault, which is I_1-type. (c) Low magnification HAADF image. The QW shows stripe contrast. The stripes are mainly on $(20\bar{2}3)$ plane, some of them are on $(10\bar{1}1)$ plane.

$In_xGa_{1-x}N$ QWs. The calculations are consistent with our experimental observation. When the thickness of InGaN layer is low (<3 nm), the QWs remains dislocation-free at such In composition. When the thickness of InGaN layer increases, the shallow facet surface evolves to roughen the surface with steeper facets such as $(20\bar{2}3)$ and $(10\bar{1}1)$. This roughening phenomenon promotes BPSF and dislocation nucleation and forms peaks and valleys in the layer.

The BPSFs and associated PDs were mainly nucleated at valleys as shown in Fig. 3. Gao and Nix have developed a model for misfit dislocation nucleation in the valleys for GeSi/Si film.[27] We propose to use this model for interpretation of BPSF and PD generation. The material in the valleys is transferred to the peaks, either through surface diffusion or sublimation condensation or effectively through reduced growth rate in the valleys. Extended defect formation within the valleys is favorable due to the higher local compressive stress and a dislocation generation is assisted by compressive stress. The formation of I_1-type BPSFs cannot occur by glide but is favored by the possible formation of $(000\bar{1})$ facets. The exposed nanofacet plane for $(20\bar{2}\bar{1})$ growth is $(000\bar{1})$, and thus BPSF formation seems more likely in $(20\bar{2}\bar{1})$ growth in comparison to $(20\bar{2}1)$ growth plane where any *c*-plane exposed nanofacet plane is likely to be (0001), although identical values for critical thickness were obtained for both $(20\bar{2}\bar{1})$ and $(20\bar{2}1)$ planes using Matthews-Blakeslee calculations. In our previous work on nonpolar and semipolar GaN growth, we have attributed BPSF formation to exposed $(000\bar{1})$ facets during growth and subsequent growth errors on these exposed facets.[28,29]

In conclusion, the microstructure of semipolar $(20\bar{2}\bar{1})$ grown InGaN SQWs for long wavelength LEDs has been examined by TEM. Interface faceting and roughening have been observed in InGaN QW; the roughening magnitude increased with QW thickness. The elastic strain distribution in InGaN layers has been found to be non-uniform even in case of thin QWs. Stress relaxation in InGaN layers grown on semipolar $(20\bar{2}\bar{1})$ GaN was realized via the formation of partial dislocations and associated with them I_1-type BPSFs. Roughened surface valleys have been demonstrated to be favorable nucleation places for BPSFs. The density of partial threading dislocations has been measured to be in the order of $10^{10}\,cm^{-2}$ that can be considered as the main detrimental factor to long wavelength LED device performance.

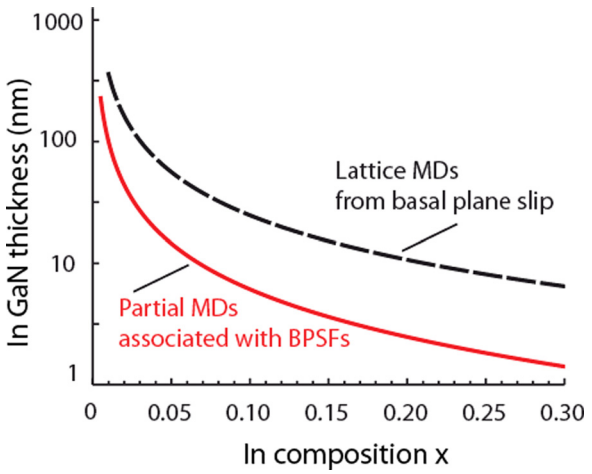

FIG. 4. Comparison of calculated critical thicknesses for MD formation in semipolar grown $(20\bar{2}\bar{1})$ $In_xGa_{1-x}N$/GaN heterostructures in cases of partial MDs associated with BPSFs of I_1-type (solid line) and lattice MDs originated from the slip in the basal plane (dashed line). To obtain the plots, the materials properties listed in Ref. 26 were utilized together with the value of $\gamma_{SF} = 0.025\,J/m^2$ for BPSF energy per unit area from Ref. 22.

The authors acknowledge the support of the Solid-State Lighting and Energy Center at UCSB and International Research Laboratory at ITMO. This work made use of Material Research Laboratory Central Facilities supported by the Materials Research Science and Engineering Centers Program of the National Science Foundation under Award No. DMR 1121053. AER was partially supported by RFBR Project No. 12-08-00397-a, and Estonian projects "NanoCom" 3.2.1101.12-0010 and IUT2-25.

[1]S. Nakamura, MRS Bull. **34**, 101 (2009).
[2]S. Yamamoto, Y. Zhao, C. C. Pan, R. B. Chung, K. Fujito, J. Sonoda, S. P. Denbaars, and S. Nakamura, Appl. Phys. Express **3**, 122102 (2010).
[3]P. Waltereit, O. Brandt, A. Trampert, H. T. Grahn, J. Menniger, M. Ramsteiner, M. Reiche, and K. H. Ploog, Nature (London) **406**, 865 (2000).
[4]F. Bernardini and V. Fiorentini, Phys. Status Solidi B **216**, 391 (1999).
[5]Y. Zhao, J. Sonada, I. Koslow, C. C. Pan, H. Ohta, J. S. Ha, S. P. DenBaars, and S. Nakamura, Jpn. J. Appl. Phys., Part 1 **49**, 070206 (2010).
[6]Y. Zhao, S. Tanaka, C. C. Pan, K. Fujito, D. Feezell, J. S. Speck, S. P. DenBaars, and S. Nakamura, Appl. Phys. Express **4**, 082104 (2011).
[7]Y. Zhao, Q. Yan, C. Y. Huang, S. C. Huang, P. S. Hsu, S. Tanaka, C. C. Pan, Y. Kawaguchi, K. Fujito, C. G. Van de Walle, J. S. Speck, S. P. DenBaars, S. Nakamura, and D. Feezell, Appl. Phys. Lett. **100**, 201108 (2012).
[8]C. C. Pan, S. Tanaka, F. Wu, Y. Zhao, J. S. Speck, S. Nakamura, S. P. DenBaars, and D. Feezell, Appl. Phys. Express **5**, 062103 (2012).
[9]R. Shivaraman, Y. Kawaguchi, S. Tanaka, S. P. DenBaars, S. Nakamura, and J. S. Speck, Appl. Phys. Lett. **102**, 251104 (2013).
[10]Y. Zhao, S. Tanaka, Q. Yan, C. Y. Huang, R. B. Chung, C. C. Pan, K. Fujito, D. Feezell, C. G. Van de Walle, J. S. Speck, S. P. DenBaars, and S. Nakamura, Appl. Phys. Lett. **99**, 051109 (2011).
[11]Y. Zhao, S. H. Oh, F. Wu, Y. Kawaguchi, S. Tanaka, K. Fujito, J. S. Speck, S. P. DenBaars, and S. Nakamura, Appl. Phys. Express **6**, 062102 (2013).
[12]F. Wu, Y. D. Lin, A. Chakraborty, H. Ohta, S. P. DenBaars, S. Nakamura, and J. S. Speck, Appl. Phys. Lett. **96**, 231912 (2010).
[13]A. Tyagi, F. Wu, E. C. Young, A. Chakraborty, H. Ohta, R. Bhat, K. Fujito, S. P. DenBaars, S. Nakamura, and J. S. Speck, Appl. Phys. Lett. **95**, 251905 (2009).
[14]P. S. Hsu, E. C. Young, A. E. Romanov, K. Fujito, S. P. DenBaars, S. Nakamura, and J. S. Speck, Appl. Phys. Lett. **99**, 081912 (2011).
[15]F. Wu, E. C. Young, I. Koslow, M. T. Hardy, P. S. Hsu, A. E. Romanov, S. Nakamura, S. P. DenBaars, and J. S. Speck, Appl. Phys. Lett. **99**, 251909 (2011).
[16]M. T. Hardy, P. S. Hsu, F. Wu, I. L. Koslow, E. C. Young, S. Nakamura, A. E. Romanov, S. P. DenBaars, and J. S. Speck, Appl. Phys. Lett. **100**, 202103 (2012).
[17]S. Yoshida, T. Yokogawa, Y. Imai, S. Kimura, and O. Sakata, Appl. Phys. Lett. **99**, 131909 (2011).
[18]T. Hanada, T. Shimada, S. Y. Ji, K. Hobo, Y. Liu, and T. Matsuoka, Phys. Status Solidi C **8**, 444 (2011).
[19]A. M. Fischer, Z. Wu, K. Sun, Q. Wei, Y. Huang, R. Senda, D. Iida, M. Iwaya, H. Amano, and F. Ponce, Appl. Phys. Express **2**, 041002 (2009).
[20]Z. H. Wu, T. Tanikawa, T. Murase, Y. Y. Fang, C. Q. Chen, Y. Honda, M. Yamaguchi, H. Amano, and N. Sawaki, Appl. Phys. Lett. **98**, 051902 (2011).
[21]D. N. Zakharov, Z. Liliental-Weber, B. Wagner, Z. J. Reitmeier, E. A. Preble, and R. F. Davis, Phys. Rev. B **71**, 235334 (2005).
[22]C. Stampfl and C. G. Van de Walle, Phys. Rev. B **57**, R15052 (1998).
[23]X. H. Wu, C. R. Elsass, A. Abare, M. Mack, S. Keller, P. M. Petroff, S. P. DenBaars, J. S. Speck, and S. J. Rosner, Appl. Phys. Lett. **72**, 692 (1998).
[24]J. E. Northrup, L. T. Romano, and J. Neugebauer, Appl. Phys. Lett. **74**, 2319 (1999).

[25]L. B. Freund and S. Suresh, *Thin Film Materials: Stress, Defect Formation and Surface Evolution* (Cambridge University Press, Cambridge, 2003), p. 396.
[26]A. E. Romanov, E. C. Young, F. Wu, A. Tyagi, C. S. Galliant, S. Nakamura, S. P. DenBaars, and J. S. Speck, J. Appl. Phys. **109**, 103522 (2011).
[27]H. Gao and W. D. Nix, Annu. Rev. Mater. Sci. **29**, 173 (1999).
[28]F. Wu, M. D. Craven, S. H. Lim, and J. S. Speck, J. Appl. Phys. **94**, 942 (2003).
[29]M. D. Craven, F. Wu, A. Chakraborty, B. Imer, U. K. Mishra, S. P. DenBaars, and J. S. Speck, Appl. Phys. Lett. **84**, 1281 (2004).